Proceedings of the First International Conference on Advanced Synthesis of Engineered Materials, San Francisco, California, 31 August-2 September, 1992

Combustion Synthesis/Densification of Ceramics and Ceramic Composites

M.A. Meyers, J.C. LaSalvia, D. Hoke, J-M. Jamet, and D.K. Kim
University of California at San Diego
La Jolla, California

Abstract

Combustion synthesis followed by densification was utilized in producing monolithic TiC and TiB_2 materials, and TiC-Ni, TiB_2-Ni, TiB_2-Al_2O_3, and TiB_2-SiC ceramic composites. Static and dynamic densification equipments were developed with the loading applied immediately after the synthesis reaction was completed and the ceramic/composite was ductile. All the ceramics exhibited an equiaxed grain structure with alternating regions at high and low dislocation densities, indicating that recovery/recrystallization mechanisms are prevalent. The grain boundaries were, as far as could be established, devoid of impurities and second phases. Quasi-static and dynamic mechanical testing were performed and revealed that the materials exhibited strength levels comparable to conventionally produced materials. Instrumented densification experiments were conducted and a temperature-dependent constitutive model was applied for plastic deformation of the porous combustion synthesis product.

Introduction

Reaction synthesis (or combustion synthesis, or SHS) is a method by which ceramics, intermetallics, alloys and their composites can be produced. The large enthalpy released when the reactants (solid, liquid, or gaseous) react results in the formation of a combustion front propagating through the material. The subject has been reviewed recently by Munir and Anselmi-Tamburini [1] and Merzhanov [2]. The mechanisms of reaction synthesis are given by Munir [3] and Yi and Moore [4]. Extensive research efforts in Russia and other countries of the former Soviet Union by Merzhanov and co-workers [5-8] have led to the industrialization of this method and to the synthesis of hundreds of materials. In the U.S., the early efforts in SHS are by Holt and Munir [9] at Lawrence Livermore National Laboratory, Niiler and co-workers [10-12] at BRL, Munir and co-workers [13] at the University of California, Davis, and K. Logan [14] at Georgia Institute of Technology. Whereas SHS has been used to produce compounds which, subsequently, are further processed (hot pressing, hot isostatic pressing) to yield monolithic compounds, the potential of using SHS in conjunction with densification and plastic deformation of the reaction products is considerable. A one-step synthesis-densification process would have significant benefits because advantage is taken of the high temperatures generated by reactions, that render ceramics workable.

At UCSD, a research effort was initiated in 1988 to dynamically densify the products of combustion synthesis using a high-speed forging machine [15-19]. This research program has yielded TiC [15, 17] and TiB_2 [16] compacts with a density higher than 96 pct of the theoretical value. In concurrence with this experimental program, the mechanical properties of TiC [15], TiB_2 [16], and TiB_2-Al_2O_3 [19] composite were assessed. TiB_2-SiC composites were also evaluated. More recently, the effort has focussed on identifying the mechanisms of deformation of the hot and porous ceramics during densification; a simple constitutive equation was successfully used. In this paper a summary of the results obtained to date is presented. The reader is referred to publications 15-18 and to the dissertations by LaSalvia [20], Hoke [21], and Jamet [22] for greater details.

Synthesis and Densification

Three basic reactions were investigated:

$$Ti + C \rightarrow TiC \quad (1)$$

$$Ti + 2B \rightarrow TiB_2 \quad (2)$$

$$3TiB_2 + 2B_2O_3 + 10Al \rightarrow 5Al_2O_3 + 3TiB_2 \quad (3)$$

Reactions (1) and (2) have been extensively studied and served as an excellent starting point. The adiabatic temperature rises are on the order of 2,000 K, with the product close to the melting point. Nickel was added in order to decrease the flow stress of the product while

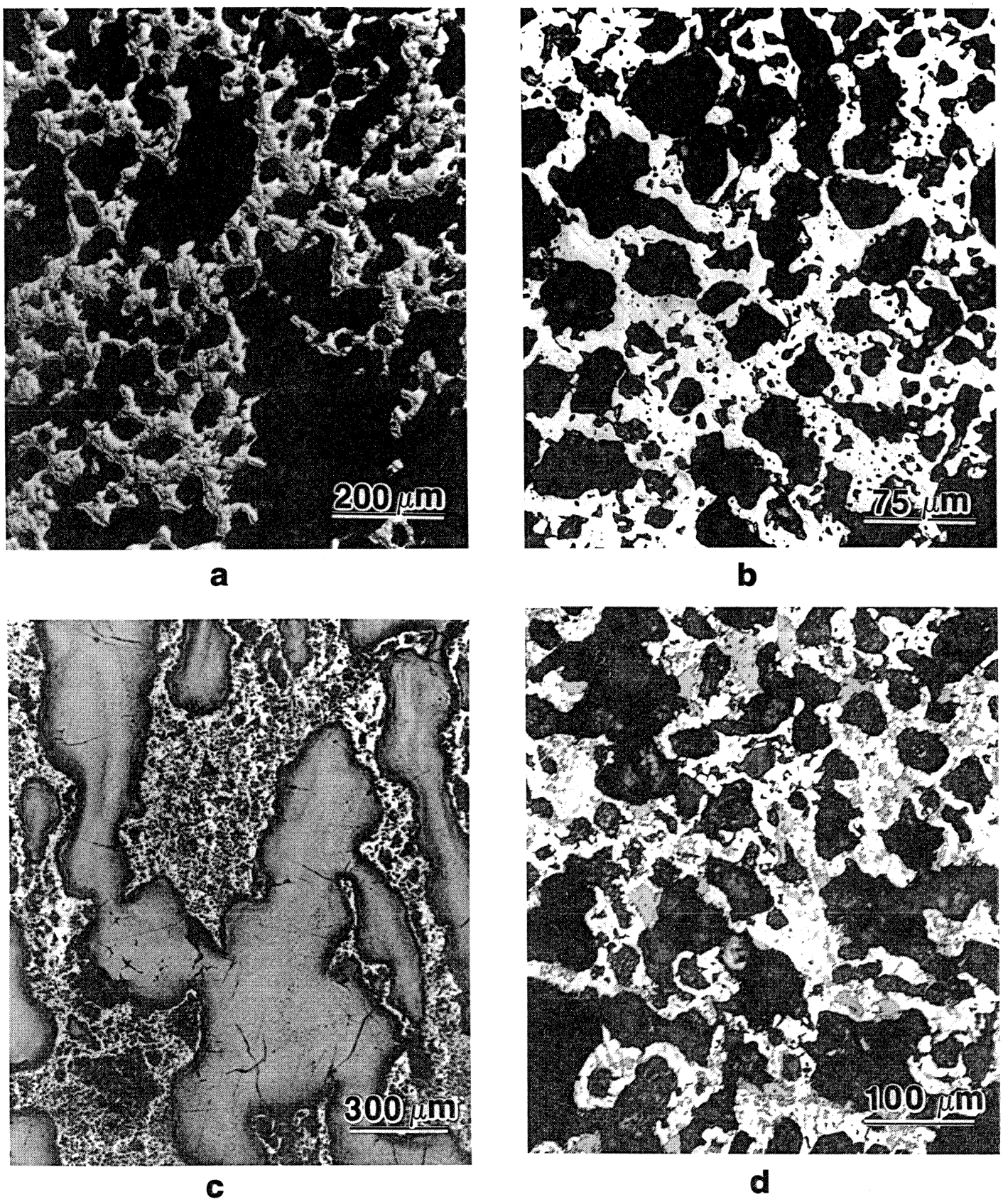

Figure 1. Porosity of as-reacted powders; (a) TiC; (b) TiB_2; (c) TiB_2-Al_2O_3; (d) TiB_2-SiC.

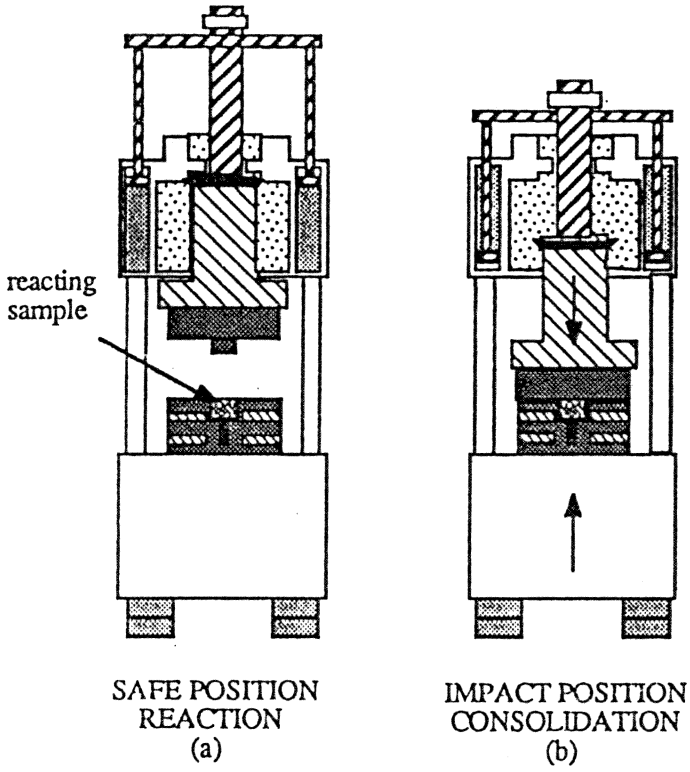

Figure 2. Sequence of events occurring during dynamic consolidation of the reaction synthesized material.

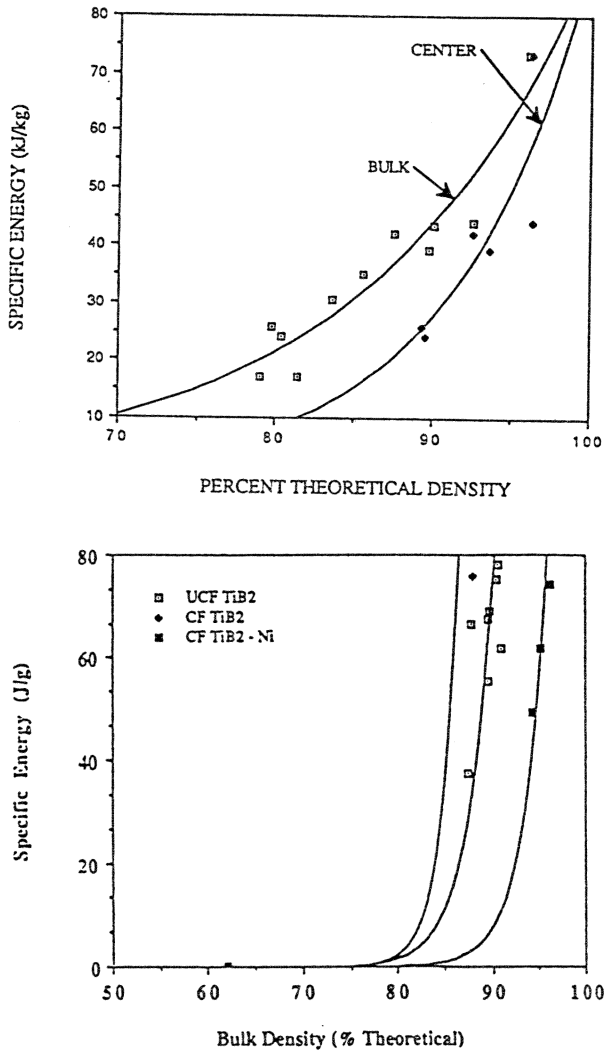

Figure 3. Bulk density achieved in high-speed forging machine as a function of specific energy for (a) TiC and (b) TiB_2, TiB_2 + inert TiB_2, and TiB_2 + Ni.

improving the properties of the products. The addition of nickel yielded very attractive microstructures and a decrease in post-densification cracking, as will be discussed in Section 3. For the Ti + 2B reaction, pre-synthesized TiB_2 was added (20%) to decrease the intensity of the reaction. And experiments are under way in which SiC powder is added to the Ti + 2B powder mixture to determine whether a composite with good interfacial properties can be made by this route. Reaction (3) uses raw materials that are technologically much more attractive than the Ti + 2B and Ti + C reactions due to the significant cost savings. The cost of B_2O_3 is only a small fraction (< 1/100) of that of boron, and TiO_2 is considerably less expensive (< 1/10) than titanium. Logan and co-workers [14] developed this reaction and applied it, in a two-stage process (SHS + grinding + hot pressing) to the production of the TiB_2-Al_2O_3 composite. The following are the particle sizes of the starting powders: Ti (< 44 μm), B (< 44 μm), C (< 2 μm), TiO_2 (0.3 μm), Al (< 20 μm), B_2O_3 (< 40 μm), Ni (< 3 μm). These powders were mixed in the stoichiometric proportions indicated by reactions 1-3 under argon atmosphere in a glove box and ball milled in a PVC jar with alumina cylindrical pellets for several hours in order to achieve homogeneity. These powder mixtures were subsequently compacted to 70% of the full density by uniaxial quasi-static pressing. Subsequent to pressing, the compacts were ignited by placing loose reactant powder on top of them and inserting in this powder an electric match. The electric current from a battery ignited the loose powder, which then transmitted the combustion wave through the compact. The products of combustion synthesis are highly porous because of three principal reasons:

(a) initial porosity of reactant mixture
(b) shrinkage associated with reaction, since products have higher density than reactants
(c) trapped gases and gas escape routes generated during combustion.

Figure 1 shows the porosity for four different combustion products. The density varies from 30 to 50 % of the theoretical value, and pores have a spherical morphology and are interconnected.

Densification within a time interval of 1-4 seconds after the completion of reaction was carried out dynamically, in a high-speed forging machine, and quasi-statically, in a uniaxial (screw-driven) mechanical testing machine. The high-speed forging machine is shown in Figure 2. This machine uses a forging hammer driven by compressed nitrogen gas, at velocities varying between 5 and 15 m/s. The forging hammer has a punch which impacts the sample, contained in a closed die and insulated from the surroundings (Figure 2(b)). Upon consolidation, the forging hammer is raised and an ejector removes the sample from the die (Fig. 2(c)). Slow cooling in a furnace was used in order to minimize thermal stresses and associated cracking. Disks with 10 cm diameter were successfully forged by this method and densities in excess of 96% of the theoretical value were obtained. The final density increased as the specific energy imparted by the hammer to the sample increased. Figure 3 shows the density of compacts as a function of machine kinetic energy. This energy is calculated by dividing the kinetic energy of hammer at the beginning of compaction by the mass of specimen. It is, of course, recognized that the conversion process is only partial and that substantial fractions of energy are transferred to the machine frame. Nevertheless, it is possible to estimate the flow stress of the hot ceramic from a simple analysis, based on the Carroll-Holt equation [23] for porous plastic materials.

$$E = \frac{2}{3\rho}\sigma_{ys}\left[\alpha_0 \ln \alpha_0 - (\alpha_0 - 1)\ln(\alpha_0 - 1) - \alpha \ln \alpha\right] \qquad \text{Eq.1}$$

E is the plastic deformation energy, α_0 and α are the initial and final distentions, respectively, (distension is defined as the ratio between the specific volumes of compact and densified material), ρ is the material density, and σ_{ys} is the flow stress of the material. This model is based on an ideally plastic material with σ_{ys} constant. For a value of the kinetic energy of the hammer of 74 J/g, and assuming a "flow efficiency" between 0.1 and 0.4 (as observed by Dorofeev and Prutsakov [24]), the values obtained from Eqn. 1 are in the range 35-150 MPa for the flow stress of TiC. The initial and final densities were taken as 0.5 and 0.96 of the theoretical value, respectively, in accordance with Figure 3(a). Dorofeev and Prutsakov [24] estimated that only between 10 and 40% of the hammer energy was absorbed by the powders. The values of flow stress for TiC reported by Katz *et al* [25] and Toth [26] are 100 MPa/1700°C and 50 MPa/1800°C, respectively. By comparing the results obtained from the Carroll-Holt [23] computation with the results of Katz *et al.* [25] and Toth [26], one may conclude that they are, to a first approximation, compatible.

The quasi-static experiments were devised to develop a better quantitative understanding of the mechanical response of the combustion synthesis products. It should be realized that quasi-static experiments are far from isothermal. Calculations conducted by Jamet [19, 22] for a 2.54-cm diameter cylinder of Al_2O_3-TiB_2 laterally insulated and confined yield the curve shown in Figure 4. For comparison purposes, the measured temperature vs. time curve for a 1.9-cm diameter TiC (+25% Ni) cylinder is plotted in the same figure; these results were obtained by Dunmead, Munir, and Holt [27]. The two curves show similar trends, and the temperature of the reacted compact is reduced to one half of its original value for a time between 25 and 80 seconds. The time interval during which the specimen is deformed in dynamic forging is approximately 0.1-0.3-seconds and the process can be assumed to be isothermal; in quasi-static testing, on the other hand, times vary between 3-30 seconds. The results of Figure 4

show that temperature drops to as high as 500°C can be observed within this time period.

Quasi-static densification experiments were performed in a screw-driven Instron machine (capactiy: 20,000 lbs.). Figure 5(a) shows the assembly. Two types of testing configurations were used: a confined test (Figure 5(a)) and a punching configuration (Figure 5(b)). Whereas the confined geometry enables a uniaxial strain experiment, cooling is rapid because of the extensive surface area of container walls and the temperature is not uniform within the specimen during testing. The punch (indentation) configuration has a much larger thermal mass and the plastic deformation process is confined to the central region. It also enables the identification of the micromechanical deformation modes, which will be discussed later in Section 4.

Microstructural Characterization

The microstructures produced may be compared with those produced with the help of SHS reactions in Dunmead *et al.* [28] and Miyamoto [29]. A brief pictorial description of the microstructures obtained is presented in this section. Optical, scanning, and transmission electron microscopy were used to characterize the materials.

Figure 6 shows the microstructure of (a) TiC and (b) TiC + 25 wt% Ni. TiC is equiaxed and some intergranular porosity is evident. The average grain size, as determined from the linear intercept, is 44 μm. The addition of 25 wt% Ni creates a continuous metallic phase enveloping the TiC grains, which acquire a spheroidal morphology. Transmission electron microscopy (Figures 7 and 8) reveals the features in greater detail. Noteworthy is the presence of dislocation arrays in some TiC particles (Figs. 7(b) and 8(a)) and their absence in nickel (Figs. 7(b) and 8(b)). The nickel phase was considerably damaged by ion milling but is shown to exhibit very large grains devoid of dislocations. The grain boundaries are clean and free of impurities; this is a positive microstructural feature.

Titanium diboride exhibited a microstructure characterized by more irregular grains, with a tendency towards greater diversity of grain size. The addition of 25 wt% inert TiB_2 powder to the reactive mixture (in order to decrease the energy evolved in reaction) undoubtedly contributed to this, and the bonding between these powders was not always optimum; Figure 9(a) shows these features with regions in which bonding is not optimum, marked by arrows. The addition of 1.5 wt% Ni resulted in significant microstructural improvement, Figure 9(b). Nickel forms a thin layer at the grain boundaries, acting as an effective binder. Transmission electron microscopy showed a mixture of annealed and deformed grains. The grain in the center part of Figure 10 is highly dislocated, while the one on the right top side is annealed. This mixture of annealed and dislocated grains seems to be indicative of recrystallization processes taking place after plastic deformation.

The product of reaction 3, $Al_2O_3 + TiB_2$, is shown in Figure 11. The two phases are characterized by a large difference in grain size and morphology. The TiB_2 phase is heterogeneously distributed in an Al_2O_3 matrix with the calculated proportions: TiB_2 (27 vol%) and Al_2O_3 (71 vol%). The TiB_2 phase is formed as clusters and long needles with a diameter of ~1 μm. The Al_2O_3 phase has a much larger grain size (on the order of 50 μm). Figure 11(a) shows a scanning electron micrograph of a fracture surface, depicting TiB_2 and Al_2O_3 phases, as indicated by A and B, respectively. Figure 11(b) shows a polished section, in which the rod-shaped TiB_2 and clusters of TiB_2 grains embedded in the Al_2O_3 matrix are clearly visible. This microstructure is characterized by a continuous Al_2O_3 phase in which TiB_2 reinforcements are embedded. Figure 12 shows transmission electron micrographs of this material. The arrays of parallel-faced grains (TiB_2) with voids (marked by arrow) are evident in Figure 12(a), while Figure 12(b) shows a dislocation array (quite an uncommon feature).

SiC (in particulate and fiber morphologies) was added to a Ti + 2B mixture in order to determine whether a reaction occurs. Figure 13(a) shows the microstructure of a mixture with 20% SiC; the darker phase is SiC and the lighter phase is TiB_2. Complete wetting at the interfaces is obtained. In some regions, a reaction between the materials occurred, resulting in a eutectic solidification with a characteristic eutectic structure shown in Figure 13(b). The addition of SiC fibers (Nicalon fibers with 12-16 μm diameter) led to reaction of these fibers and the dissolution and re-emergence of SiC. Figure 13(c) shows darker circular regions which are the traces of the original fibers; the TiB_2 matrix (lighter phase) is interspersed with SiC that originated from the dissolution of fibers in the matrix. In Figure 13(d) these fibers have lost the original circular shape. Figures 13(a)-(d) show the good wetting between the two phases that predict superior mechanical properties. The evaluation of these properties is currently under way.

Constitutive Modeling of Densification

In Section 2 two quasi-static densification configurations are described (Figure 5): the confined densification and the punch-shearing geometries. Whereas the punch (indentation) configuration of Figure 5(c) is currently being developed and implemented, a number of experiments have been conducted on the confined configuration which yielded, through analysis, a flow stress dependence of temperature for the Al_2O_3-TiB_2 ceramic composite. The results are presented in greater detail by Jamet [19, 22] and are summarized here.

A typical stress vs. density plot for the densification of TiB_2-Al_2O_3 is shown in Figure 14(a). Three distinct densification regions can be identified. At first, the increase in density at very low values of stress corresponds to both compression of the loose powder

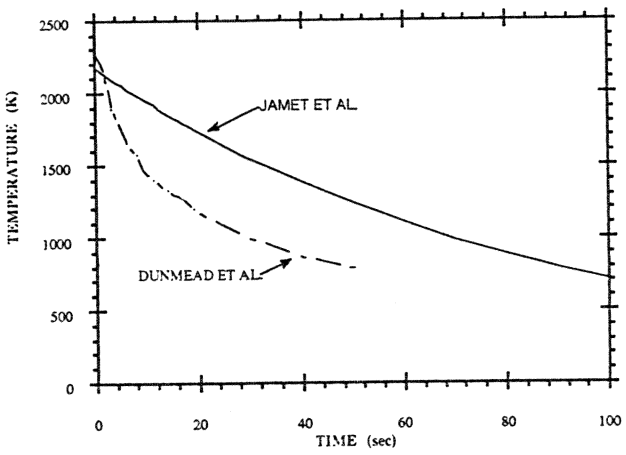

Figure 4. Calculated and measured (by Dunmead *et al.* [27]) temperature as a function of time for cylindrical compact with 2 - 2.5 cm diameter.

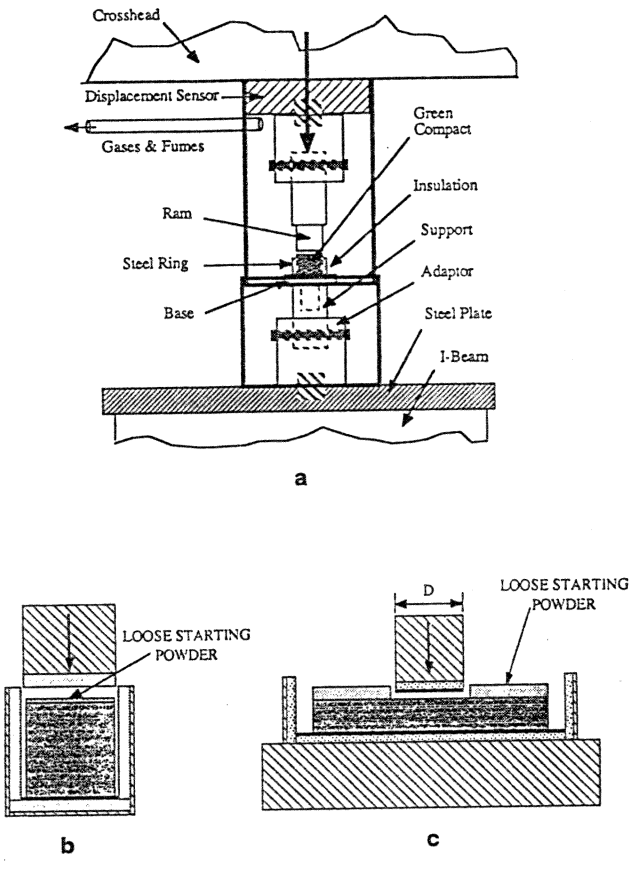

Figure 5. (a) Quasi-static densification set-up in uniaxial testing machine; (b) and (c) powder testing configurations.

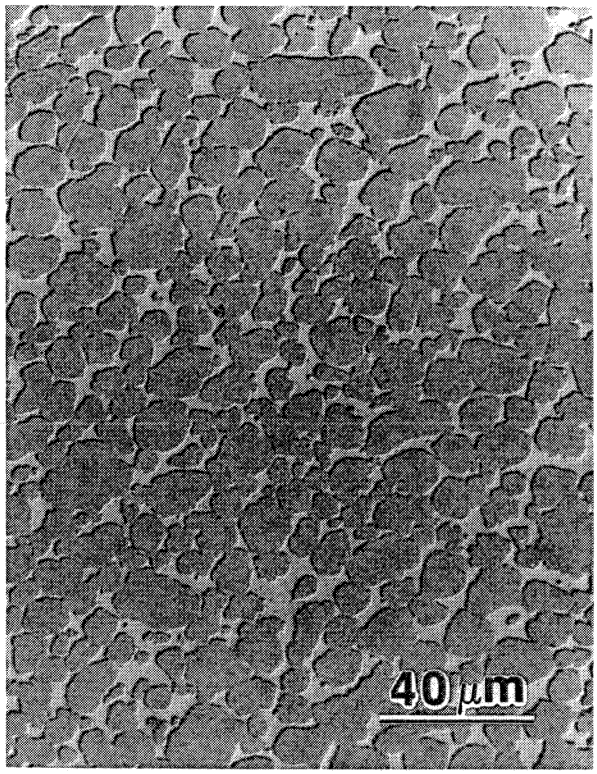

Figure 6. Microstructure of combustion synthesized/ dynamically compacted (a) TiC and (b) TiC + 25 wt.% Ni.

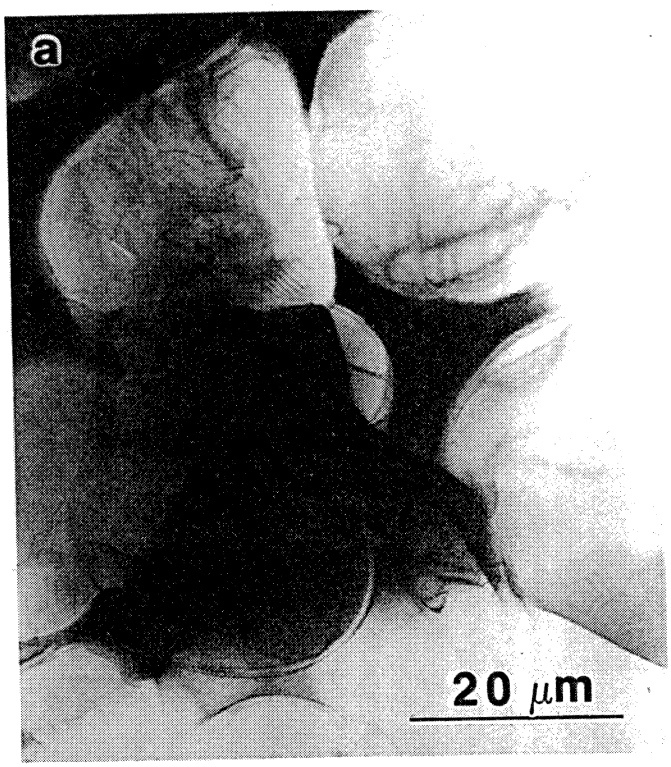

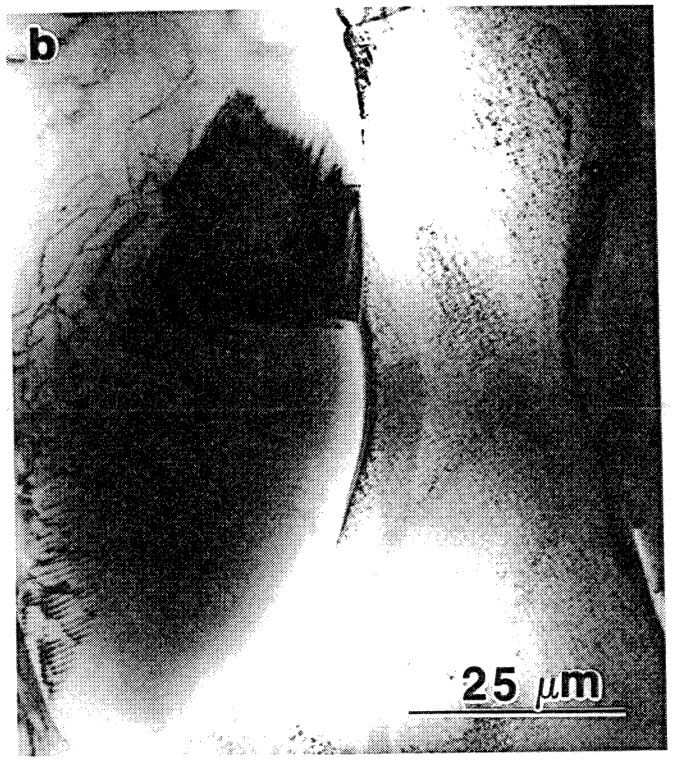

Figure 7. Transmission electron micrograph of TiC + 20% Ni showing (a) spheroidal TiC grains and (b) dislocations within TiC.

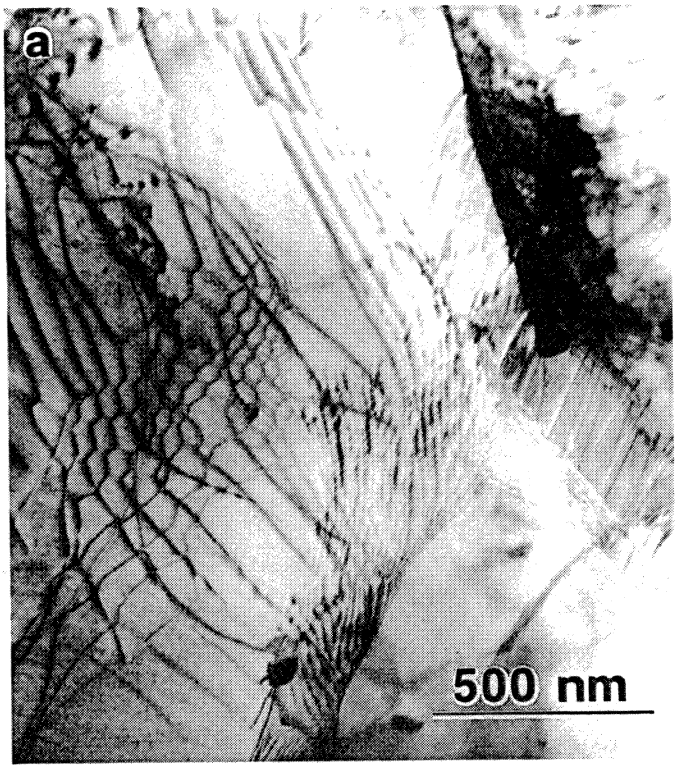

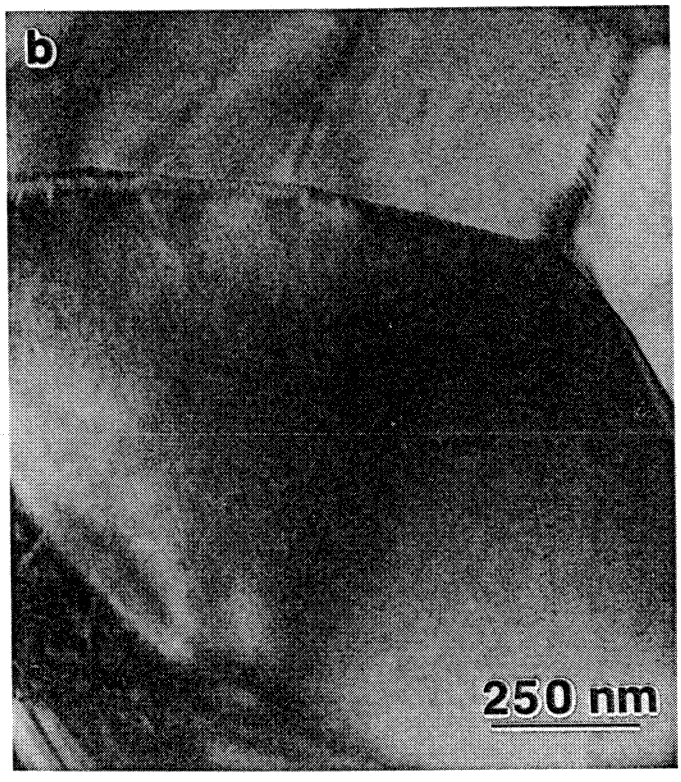

Figure 8. Transmission electron micrograph of TiC + 20% Ni showing (a) dislocation network in TiC grain and (b) Ni-Ti-C boundary (arrow).

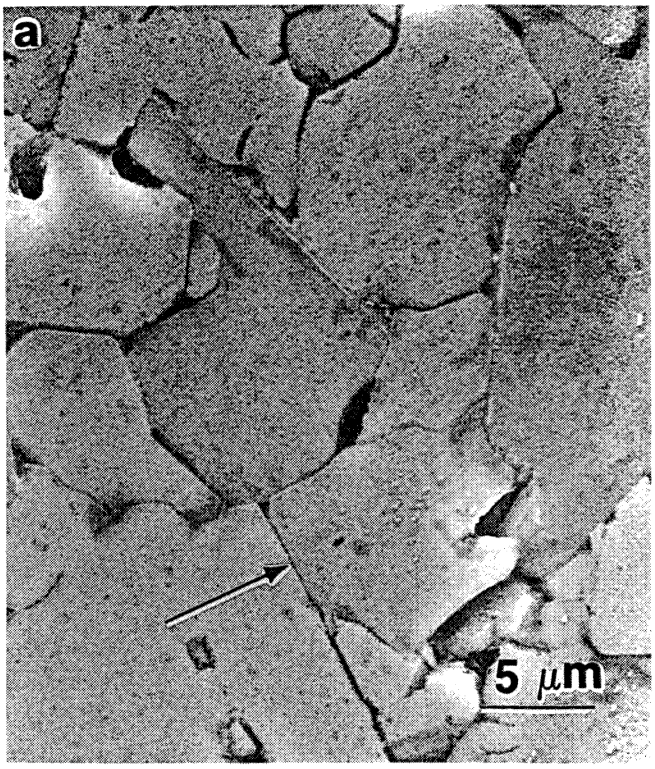

Figure 9. Microstructure of combustion synthesized/ dynamically compacted (a) TiB_2 and (b) TiB_2 + 1.5 Ni.

Figure 10. Transmission electron micrograph of TiB_2 showing grain with dislocations.

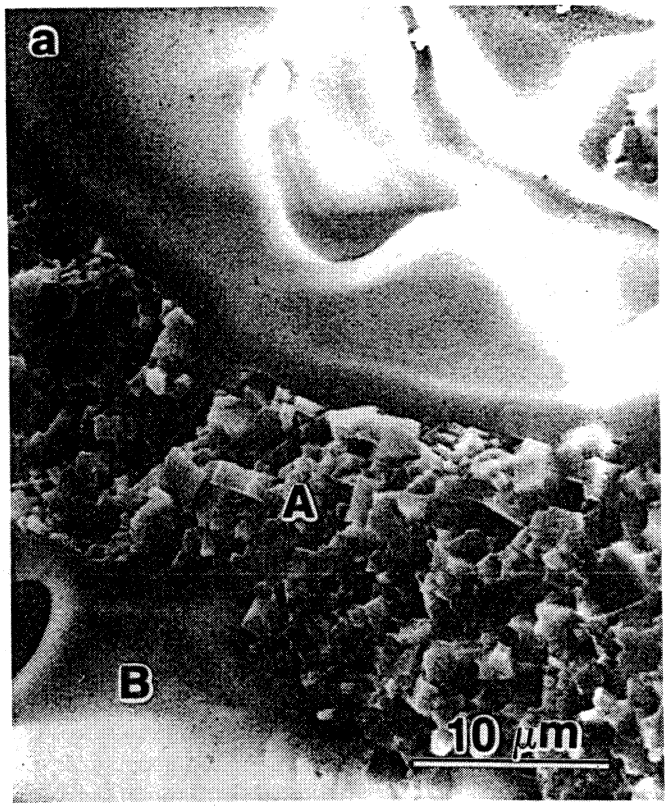

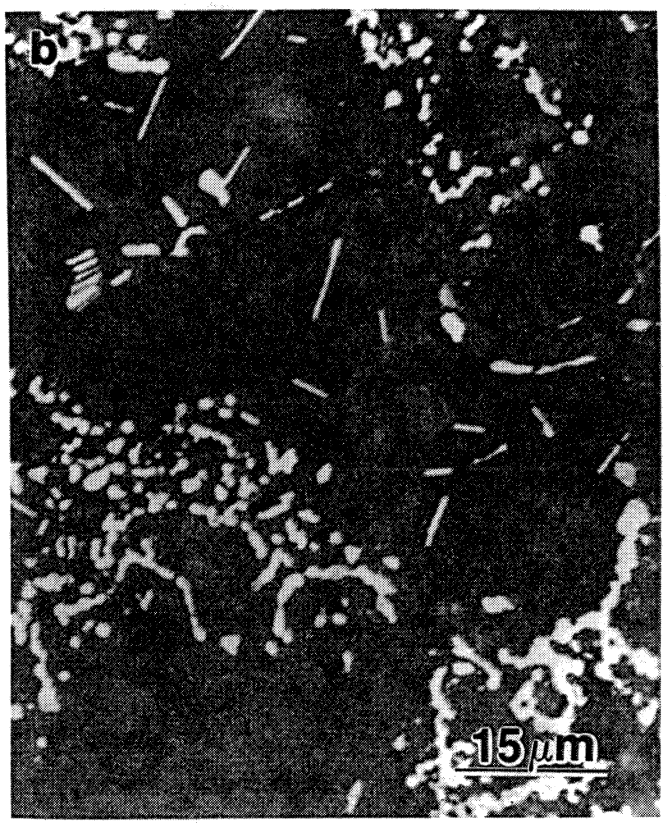

Figure 11. (a) Scanning electron micrographs of fracture surface showing TiB_2 and Al_2O_3 phases; (b) optical micrograph showing dispersion of needle-shaped TiB_2 grains in the Al_2O_3 matrix.

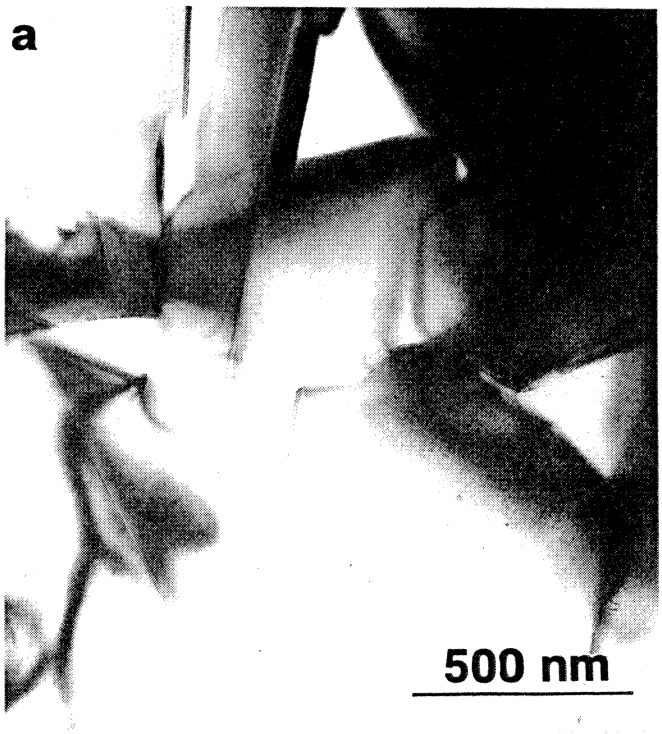

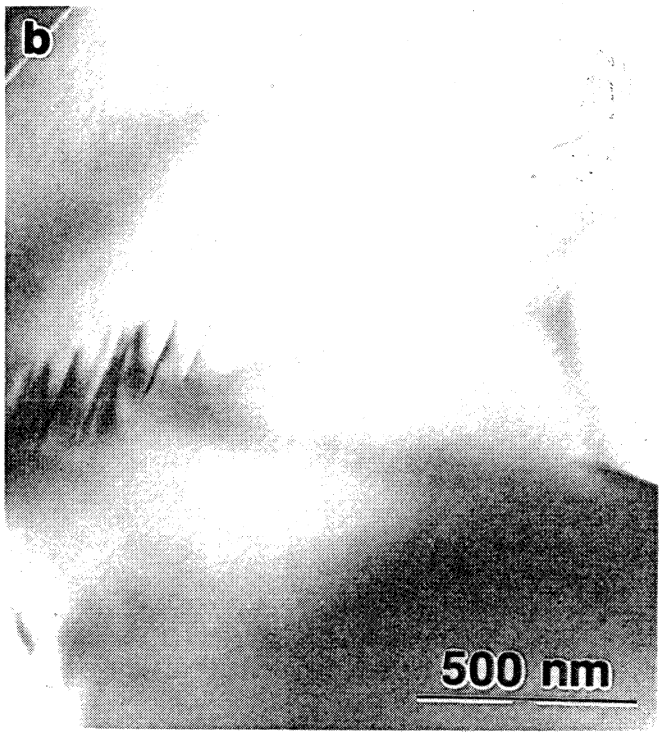

Figure 12. Transmission electron micrographs of Al_2O_3-TiB_2 composite; (a) geometrical array of TiB_2 grains; (b) dislocation arrays in grain.

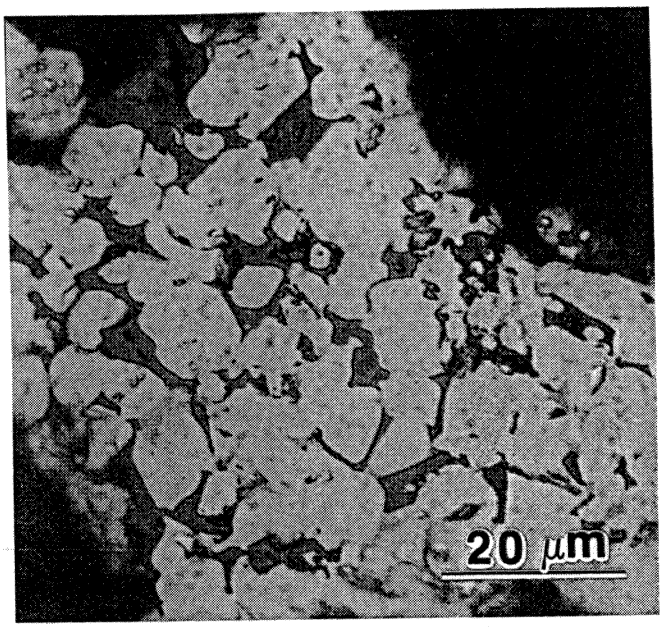

a

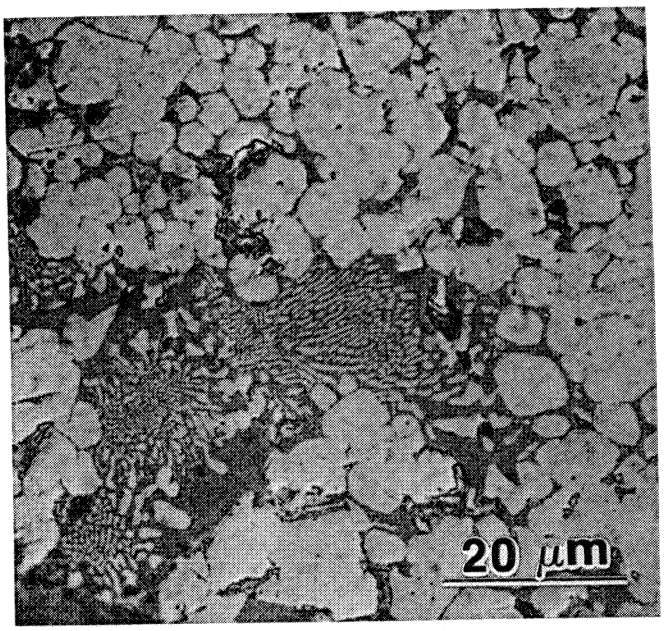

b

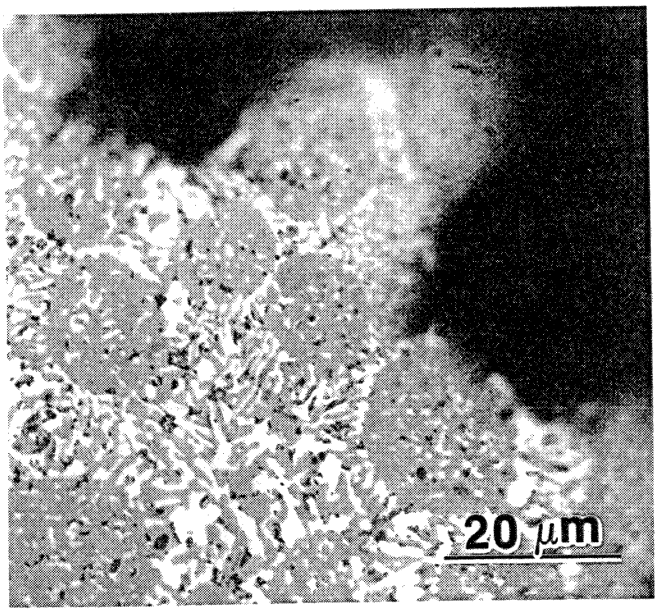

c

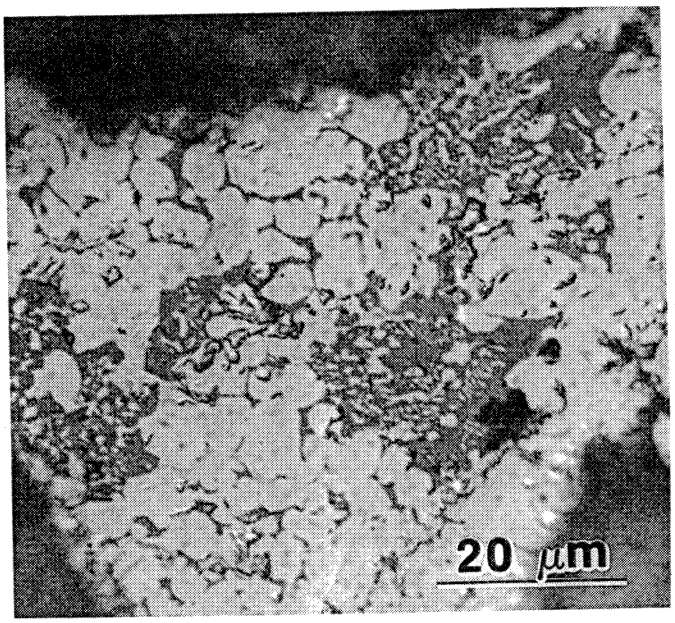

d

Figure 13. Microstructures of combustion synthesized TiB_2 (from Ti + 2B reaction) and SiC; (a) and (b) addition of 20% particulate SiC; (c) and (d) addition of 20% fiber.

added for ignition on top of the sample and the collapse of the large flaky pore structure at high temperature (region I). The slope of this range is very low. In an intermediate stage (region II), stress starts increasing regularly with density. This region can be attributed to the end of the collapse of the largest pores combined with the beginning of smaller pore elimination while temperature is decreasing. The final stage (region III) corresponds to the collapse of the small pore structure accompanied by stiffening of the bulk material (temperature drops due to heat losses). In that region, stress dramatically increases when density reaches high values. The effect of strain rate can be clearly seen in Figure 14(b) where the slope of the stress-strain curve increases with decreasing values of strain rate. Tests at lower strain rate last longer, implying more heat losses, a lower temperature, and attendant stiffening of the material. Stress therefore reaches a higher value for the same amount of strain.

By comparing the observed and predicted uniaxial strain compression behavior (using a modified densification model of the hot porous material in which a temperature dependent flow stress is incorporated), it is possible to obtain a preliminary value and to approximate the variation of the flow stress of porous TiB_2-Al_2O_3 with temperature.

The general expression of the yield criterion for ductile porous materials in an isothermal experiment is:

$$AJ_2 + BI_1^2 = \delta Y_0^2 = Y_R^2 \qquad \text{Eq. 2}$$

where different expressions have been proposed for A, B, and δ in terms of relative density. J_2 is the second invariant of deviatoric stress component and I_1, the first invariant of the stress tensor. Y_0 is the yield stress of the fully dense material, and Y_R its yield stress at corresponding relative density R. For the specific case of uniaxial strain compression (repressing) of an axisymmetric body, it is assumed that $d\varepsilon_r = d\varepsilon_\theta = 0$ and $\sigma_r = \sigma_\theta = [\nu/(1-\nu)]\sigma_z$ (ν being Poisson's ratio of the material).

For porous materials, Kuhn and Downey [30] found the relationship between R and ν to be $R^2 = 2\nu$. In the model they proposed, $A = 2 + R^2$ and $B = (1 - R^2)/3$, and $\delta = 1$. The yield criterion is then given by :

$$\sigma_z(R) = Y_0\left[\frac{(2 - R^2)}{(1 - R^2)(2 + R^2)}\right]^{\frac{1}{2}} \qquad \text{Eq. 3}$$

On the other hand, Doraivelu *et al.* [31] introduced the dependence of yield stress on relative density via a δ term :

$$\delta = \frac{R^2 - R_c^2}{1 - R_c^2} \qquad \text{Eq. 4}$$

According to that model, the critical density (R_c) where the compact loses all mechanical strength was chosen to be the density at the beginning of consolidation, $R_c \approx 0.4$ (40% of the products' theoretical density). Such a choice was made because of the presence of a liquid phase during the reaction (T_{ad} = 2175°C) for the TiB_2-Al_2O_3 system and the first stage of compaction (before solidification of the alumina phase at T_{am} = 2080°C).

A temperature dependence must be added to Doraivelu's modification [31] of the Kuhn and Downey [30] equation and Y_0 has to be replaced by a temperature dependent term Y(T). As a first approximation, it is assumed that the dependence of yield stress on temperature is given by :

$$Y(T) = Y_0\left(1 - \frac{T - T_0}{T_{am} - T_0}\right) \qquad \text{Eq. 5}$$

where Y_0 is a "pseudo" yield stress at T_0 = 25 °C, the room temperature. Since the liquid alumina phase exists until T_{am} = 2080 °C, the flow stress can be assumed to be zero between the adiabatic temperature T_{ad} and T_{am}.

The stress-density relationship describing the hot porous material behavior during consolidation that includes the effect of temperature is obtained by substituting equation (5) into the modified form of (3) :

$$\sigma_z(R,T) = Y_0\left(1 - \frac{T - T_0}{T_{am} - T_0}\right)\left(\frac{R^2 - R_c^2}{1 - R_c^2}\right)^{\frac{1}{2}}\left[\frac{(2 - R^2)}{(1 - R^2)(2 + R^2)}\right]^{\frac{1}{2}}$$

Eq. 6

Equation (6) depends explicitly on temperature and density, and also implicitly on time via T and R. The temperature as a function of time was obtained by Jamet [19, 22] and is shown in Figure 4. It is analytically expressed as:

$$T = 25 + 2150 \exp(-0.0114t) \qquad \text{Eq. 7}$$

The Y_0 value was adjusted in order to match the experimental curves; shown in Figure 15(a), where both the model and experiment are represented, is an example of good agreement for a typical quasi-static consolidation. The "pseudo" yield stress Y_0 that matches the experimental results is 1.07 GPa. The evolution of the yield stress within the temperature range of the quasi-static consolidation experiments (1940-2175°C) is shown in Figure 16. Ramberg and Williams [32] reported the yield stresses of TiB_2 as a function of temperature. The values obtained from the model developed here are fairly consistent with the results interpolated from Ramberg and Williams' [32] data for TiB_2. The value for Y_0 that fits the experimental results best is somewhat artificial, because TiB_2 and Al_2O_3 do not undergo plastic deformation at room temperature and fail by fracture. The

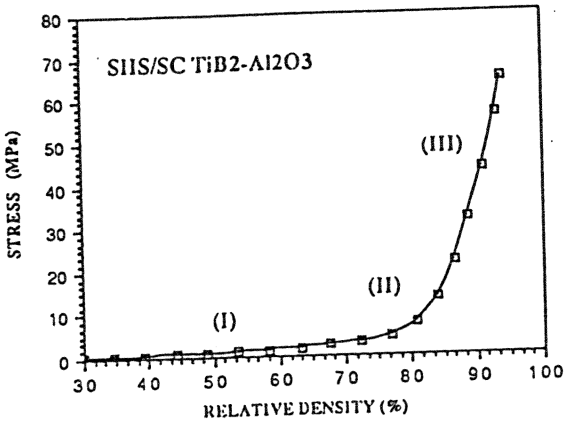

a

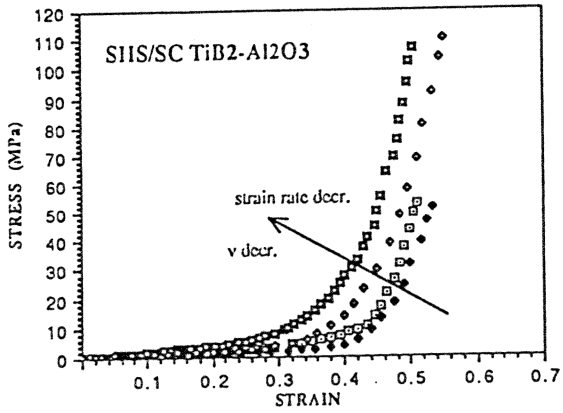

b

Figure 14. (a) Typical stress-density curve for the consolidation of TiB_2-Al_2O_3. (b) Stress-strain curves for quasi-static compaction of TiB_2-Al_2O_3 samples showing the effect of strain rate.

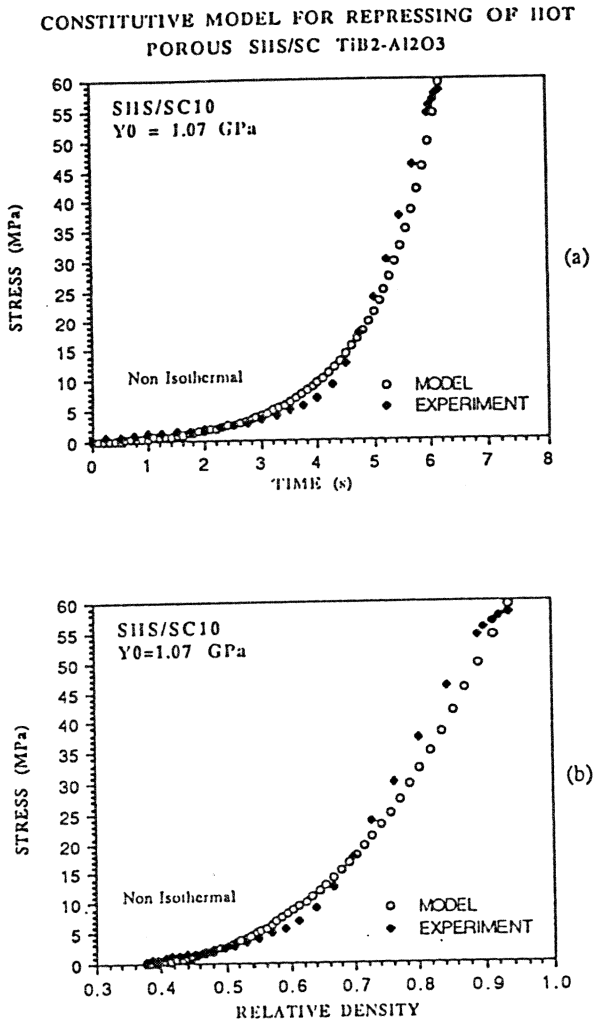

Figure 15. Comparison of the constitutive model for axial strain compression (repressing) of hot porous TiB_2-Al_2O_3 and the corresponding experimental curve. (a) stress vs. time, and (b) stress vs. relative density.

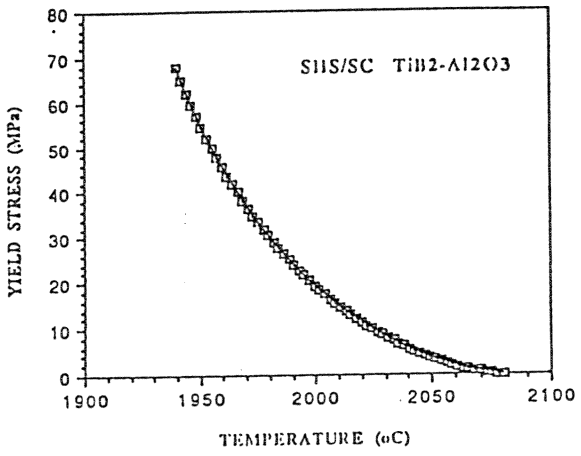

Figure 16. Yield stress as a function of temperature for TiB_2-Al_2O_3 during quasi-static consolidation.

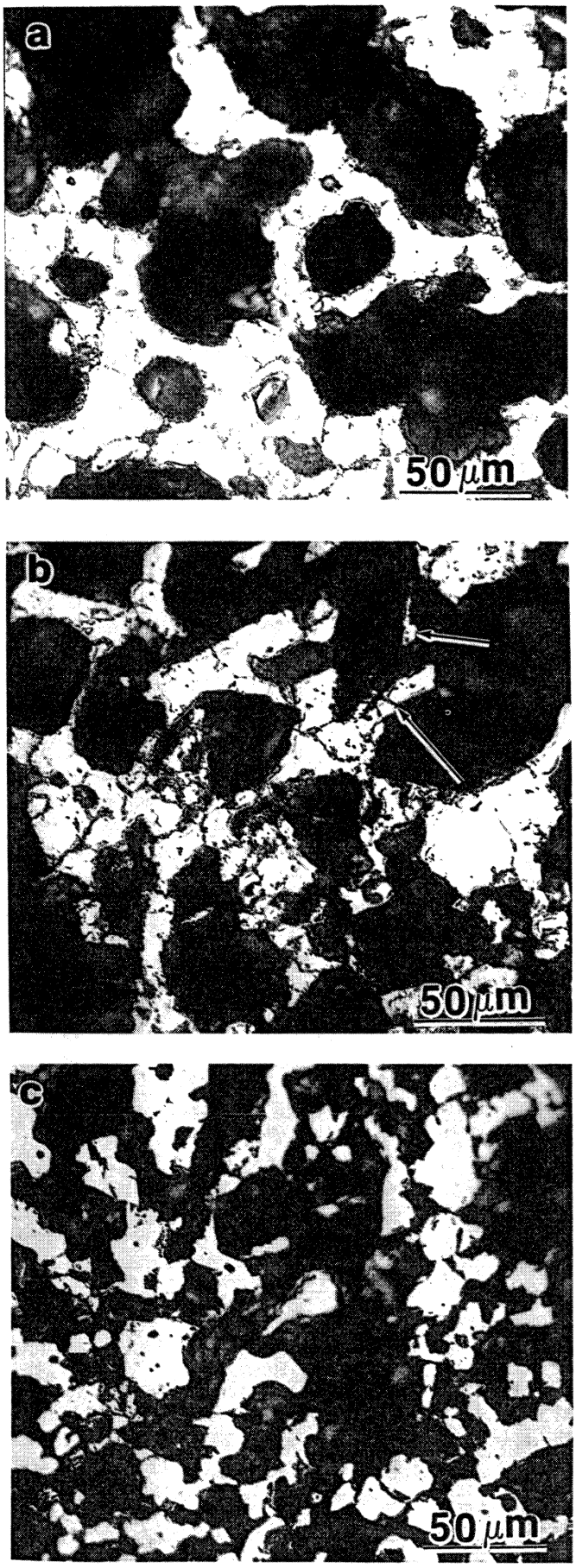

Figure 17. Cell structure of TiC and its break-up in quasi-static indentation test; (a) original cell structure; (b) fracture of cell webs; (c) fractured cell structure during densification.

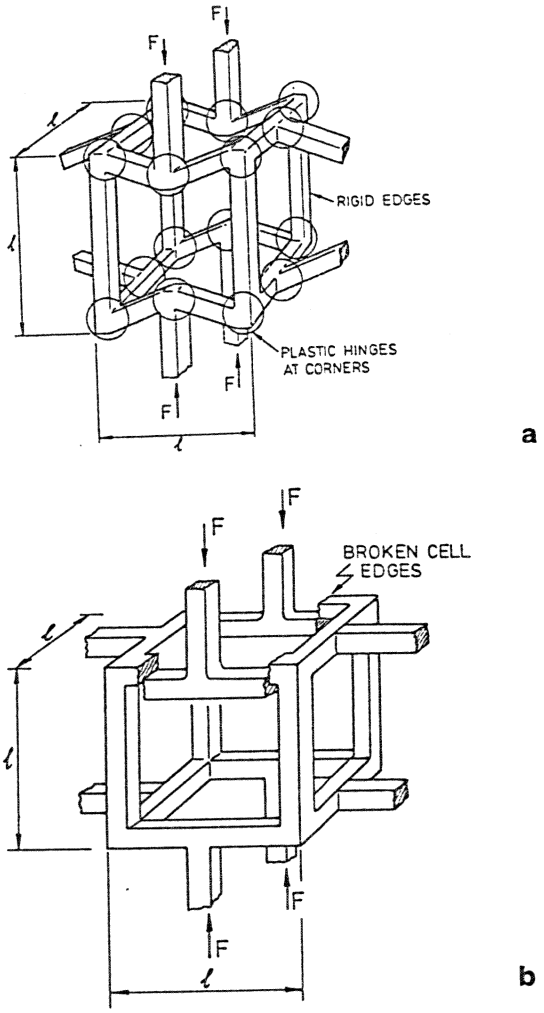

Figure 18. Simplified model for cell structure and (a) its plastic deformation and (b) break-up during densification (From L. J. Gibson and M. F. Ashby, *Cellular Solids*, Pergamon, 1988, pp. 143, 149).

compressive strength of this TiB_2-Al_2O_3 composite would be closer to 4 GPa.

Preliminary tests were conducted using the punch test shown in Figure 5(c). The temperature drop during this test is much less significant. Interrupted densification tests enabled the identification of the densification mechanism. Figure 17 shows results from an interrupted experiment. The cell structure is intact in regions far from the punch and is totally destroyed under the punch. There is a region where the cell break up mechanism could be identified. This is shown in Figure 17(b). Sites, where the cell walls are fractured, are identified by arrows. Thus, the deformation mechanism in the TiC specimen investigated was one of brittle fracture of the cells and their subsequent densification. This indicates that the material was at a temperature below the ductile-to-brittle transition while being deformed. These observations do not preclude ductile deformation, if the temperature is sufficiently high. Gibson and Ashby [33] have developed models for the elastic, plastic and fracture behaviors of cellular materials. Based on their analysis, it is possible to propose a mechanism for the "crush-up" process. Gibson and Ashby [33] considered two types of cells in foams: open cells and closed cells. The necessity of paths for the escape of gases in the combustion synthesis process indicates that the open cell is a better model. Figure 18 shows the simple model devised by Gibson and Ashby for open cells: they consist of beams with square cross sections arranged in an orthogonal pattern. Plastic deformation occurs by beam bending (Figure 18(a)), while crushing occurs by fracture of the beams (Figure 18(b)) The dimensions of the beam (l and t) are related to the density of the porous material by:

$$\frac{\rho_f}{\rho_s} = \left(\frac{t}{l}\right)^2 \qquad \text{Eq. 8}$$

ρ_f and ρ_S are the foam and solid density, respectively, and t and l are the beam thickness and length, respectively. The foam shown in Figure 17 has a characteristic length (l) of approximately 50 μm. Since the initial density of the material is ~0.5 ρ_S, t is approximately equal to 35 μm. Gibson and Ashby [33] obtained the flow and fracture stresses of the foam by applying mechanics principles to the geometries of Figure 18. For plastic deformation, they arrived at:

$$\frac{\sigma_f}{\sigma_{ys}} = 0.23\left(\frac{\rho_f}{\rho_s}\right)^{3/2}\left[1 + \left(\frac{\rho_f}{\rho_s}\right)^{1/2}\right] \qquad \text{Eq. 9}$$

If the process is one of break-up of the cells, such as the one shown in Figure 17(c), then Gibson and Ashby [33] have the following equation:

$$\frac{\sigma_f}{\sigma_{fs}} \simeq 0.65\left(\frac{\rho_f}{\rho_s}\right)^{3/2} \qquad \text{Eq. 10}$$

Here, σ_{fs} is the modulus of rupture, or the maximum tensile stress that the surface of a beam exhibits at the fracture point. Work is currently under way on the extension of the simple Gibson-Ashby model to foams exhibiting a distinction of cell sizes.

Conclusions

The densification of the products of combustion synthesis was carried out quasi-staticaly and dynamically. Immediate densification upon the completion of the reaction was implemented leading to high densities (> 96%). This process benefits from the high rate of load application because of the minimization of heat losses. Progress is being made towards development of microstructurally-based constitutive description of the densification process.

Acknowledgements

This research was supported by the U. S. Army Research Office under Contract No. ARO-DAAL-03-88-K-0194 and the National Science Foundation under Grant No. CBT 8713258. The help provided by Dr. K. Logan and Mr. G. Villa-Lobos from Georgia Tech. Research Institute, in providing the starting materials and demonstrating their use to us is greatly acknowledged. Discussions with Dr. A. Niiler, from the U.S. Army Ballistic Research Laboratory, were very important to the success of this program. At U.C. San Diego, we gratefully acknowledge the help provided by Mr. K. Bluegell and Mr. L.H. Yu.

References

1. Z.A. Munir and U. Anselmi-Tamburini, *Mater. Sci. Rep.* **3** (1989) 281.
2. A.G. Merzhanov: in *Combustion and Plasma Synthesis of High-Temperature Materials*, eds., Z.A Munir and J.B. Holt, VCH Publishers, New York, NY, 1990, p.1.
3. Z A. Munir, *Met. Trans. A* **23A** (1992) 7.
4. H. C. Yi and J. J. Moore, *J. Mater. Sci.* **25** (1990) 1159.
5. E. I. Maksimov, A. G. Merzhanov, and V. M. Shkirko, *Comb. Expl. Shock Waves* **1** (1965) 15.
6. N. P. Novikov, I. P. Borovinskaya, and A. G. Merzhanov, "Thermodynamic Analysis of Self-Propagating High-Temperature Synthesis Reactions," in *Combustion Processes in Chemical Technology and Metallurgy*, ed. A. G. Merzhanov, Chernogolovka, 1975 (English Translation).
7. V. M. Maslov, I. P. Borovinskaya, and A. G. Merzhanov, *Comb. Explo. Shock Waves* **12** (1976) 631.
8. Y. M. Maksimov, A. T. Pak, G. B. Lavrancuk, Y.S. Naviborodenko, and A. G. Merzhanov, *Comb. Explo. Shock Waves* **15** (1979) 415.

9. J. B. Holt and Z.A. Munir, *J. Mater. Sci.* **21** (1986) 256.
10. A. Niiler, T. Kottke, and L. Kecskes, "Shock Consolidation of Combustion Synthesized Ceramics," in *Proc. First Workshop on Industrial Applications of Shock Processing of Powders*, New Mexico Tech., Socorro, NM (1988) 901.
11. A. Niiler, L.J.Kecskes, T. Kottke, P.H. Netherwood, Jr., and R.F. Benck, "Explosive Consolidation of Combustion Synthesized Ceramics: TiC and TiB_2," *Ballistic Research Laboratory Report* BRL-TR-2951, Aberdeen Proving Ground, MD, December 1988.
12. A. Niiler, L. J. Kecskes, T. Kottke, in *Shock-Wave and High-Strain-Rate Phenomena in Materials*, eds. M. A. Meyers, L.E. Murr, and K. P. Staudhammer, M Dekker, NY, 1992, p. 293.
13. Z.A. Munir, *Am. Ceram. Soc. Bull.* **67** (1988) 343.
14. K.V. Logan, J.T. Sparrow, and W.J.S. McLemore, in *Combustion Synthesis of High-Temperature Materials*, eds. Z.A. Munir and J.B. Holt, VCH Publishers, NY, 1990, p. 219.
15. J.C. LaSalvia, L.W. Meyer, and M.A. Meyers, *J. Am. Ceram. Soc.* **75** (1992) 592.
16. D.A. Hoke, M.A. Meyers, L.W. Meyer, and G.T. Gray III, *Met. Trans.* **23A**, (1992) 77.
17. K. S. Vecchio, J. C. LaSalvia, M. A. Meyers, and G. T. Gray III, *Met. Trans.* **23A** (1992) 87.
18. J. C. LaSalvia, L. W. Meyer, D. Hoke, A. Niiler, and M. A. Meyers, in *Shock-Wave and High-Strain-Rate Phenomena in Materials*, eds. M. A. Meyers, L. E. Murr, and K. P. Staudhammer, M Dekker, NY, 1992, p. 261.
19. J. M. Jamet and M. A. Meyers, *Met. Trans.*, submitted for publication, 1992.
20. J. C. LaSalvia, "Production of Dense Titanium Carbide by Combining Reaction Synthesis with Dynamic Consolidation," M.Sc. Thesis, University of California, San Diego, 1990.
21. D. A. Hoke, "A Study on the Reaction Synthesis and Dynamic Compaction of Titanium Diboride by a High Speed Forging Machine," M.Sc. Thesis, University of California, San Diego, 1991.
22. J. M. Jamet, "Study of the TiB_2-Al_2O_3 Composite Produced by Reaction Synthesis Followed by Dynamic or Quasi-Static Compaction," M.Sc. Thesis, University of California, San Diego, 1992.
23. M. M. Carroll and A. C. Holt, *J. Appl. Phys.* **43** (1972) 1626.
24. Y. G. Dorofeev and V. T. Prutsakov, *Sov. Powder Metall. Met. Cer.* (English Translation) **11** (1972) 191.
25. A. P. Katz, H. A. Lipsitt, T. Mah, and M. G. Mendiratta, *J. Mater. Sci.* **18** (1983) 1983.
26. L. E. Toth, *Transition Metal Carbides and Nitrides*, Academic Press, New York, 1971, pp. 169-176.
27. S. D. Dunmead, Z. Munir, and J. B. Holt, *J. Am. Cer. Soc.* **75** (1992) 175.
28. S. D. Dunmead, D. W. Ready, C. E. Demler, and J. B. Holt, *J. Am. Cer. Soc.* **89** (1992) 321.
29. Y. Miyamoto, *Bull. Am. Cer. Soc.* **69** (1990) 686.
30. H. A. Kuhn and C.L. Downey: *Int. J. Powd. Met.* **7** (1971) 15.
31. S. M. Doraivelu, H.L. Gegel, J.S. Gunasekera, J.C. Malas, J.T. Morgan, and J.F. Thomas, Jr., *Int. J. Mech. Sci.* **26** (1984) 527.
32. J. R. Ramberg and W. S. Williams, *J. Mater. Sci.* **22** (1987) 1815.
33. L. J. Gibson and M. F. Ashby, *Cellular Solids*, Pergamon, 1988.